**Proceedings of ASME Turbo Expo 2011**
**GT2011**
**June 6-10, 2011, Vancouver, British Columbia, Canada**

**GT2011-45777**

# TIME-ACCURATE CALCULATIONS OF A PASSIVE SHROUD BLEED CONFIGURATION AND IMPLICATIONS FOR UNSTEADY BLADE LOADING

**Xiangyang Deng**
United Technologies Research Center (China) Ltd.
Room 3512, 35/F, Shanghai World Financial Center, 100 Century Avenue, Pudong, Shanghai, 200120, P.R.China

**Elizabeth A. Lurie**
United Technologies Research Center
411 Silver Lane, East Hartford, CT 06108, USA

**Jinzhang Feng**
United Technologies Research Center
411 Silver Lane, East Hartford, CT 06108, USA

## ABSTRACT

A time-accurate simulation of the flow through a centrifugal compressor stage consisting of a radial inlet with bleed air injection holes, an impeller with air bleed exit holes, and vaneless diffuser is performed for the peak efficiency and near-stall conditions to address fundamental questions regarding the time-varying flowfield. Unsteady results at near-stall point are compared to three steady-state simulations: (1) a simulation without recirculating bleed air at near-stall point; (2) a simulation with axisymmetric slot bleed at near-stall point; and (3) a simulation without recirculating bleed air at an increased inlet mass flow rate that accounts for the additional throughflow associated with the amount of bleed air. By these analyses, it is established that representing the bleed flow as axisymmetric, hence steady state in the rotating frame of reference, provides assessment of the time-average compressor performance; that the time-average loading is similar in both qualitative and quantitative manner to the steady state model; that the unsteady blade loading is dominated by first and second harmonic of bleed hole passing frequency and of similar magnitude to mean loading; and that the blade hole alters the local blade loading as far down as 60% span.

## INTRODUCTION

### Background

Due to its simplicity and high single stage pressure ratio, centrifugal compressors are favored for applications such as turbochargers and auxiliary power units. In these applications, one of major challenges is to extend the operation range so that the compressor is able to function throughout the entire operation envelop while keeping good fuel consumption. Different techniques have been developed to broaden the centrifugal compressor operational range, which were categorized by Rodgers [1] into mechanical methods and aerodynamic methods. The former primarily refers to variable IGV and variable diffuser [2, 3]. The latter involves endwall treatment, shroud bleed, diffuser leading edge and end gap treatment [4, 5, 6].

Shroud bleed or ported shroud, as a simple passive control device, is very effective to extend the operational range. Fig.1 shows the layout of a typical ported shroud, where bleed slots are arranged circumferentially along the inducer shroud region and communicate with the injection holes in the bellmouth shroud through the settling plenum. This configuration not only shifts the compressor surge line to a lower flow rate by bleeding high pressure air from inducer passage to the inducer leading edge, thus mitigating incidence angle to delay the inducer stall during low-airflow operation, but also increases the choke flow rate during high mass flow operation due to this bypass. Many studies on ported shroud technique were conducted in the past five years. Slovisky et al. [7] investigated the effects of both axisymmetric bleed slot width and streamwise location on the centrifugal impeller performance using design of experiment (DOE) coupled with CFD modeling. Their results indicate that the stall point varies somewhat at different slot widths and streamwise locations, but all of the configurations demonstrate adequate stall margin improvement. Moreover, they proposed that achieving rapid static pressure rise across the slot is a key to obtain good performance for the ported shroud compressor. A similar DOE approach combined with CFD modeling was also used by Yin et al [8] for a turbocharger compressor with ported shroud housing. The final results indicate that the distance between the optimal bleed slot streamwise location and impeller leading edge is about 17.5% blade tip pitch length. Ishida et al [9] performed a numerical investigation into a moderate specific speed impeller and concluded that the bleed slot in the inducer region should be located near the inducer tip throat, and that modifying the slot edge with a corner radius may give better impeller performance at large flow rate conditions. Later, Ishida et al [10] developed a ported shroud arrangement with inside guide vanes to control the swirl intensity of the recirculating bleed air and achieved 53% reduction of unstable flow range without deterioration of the impeller characteristics over the entire operation range. Similar results were also obtained by Tamaki et al [11] from both CFD and test studies into a 5.7:1 pressure ratio turbocharger compressor, where the surge margin using ported shroud and guide vanes is extended more than 10%, with no efficiency penalty at design point compared to the case without guide vanes in the bleeding system. The surge margin in their study is defined as $(Q_0-Q_s)/Q_0$, where $Q_0$ is the design volume flow rate and $Q_s$ is the volume flow rate at the surge point with the pressure ratio equal to the design pressure ratio in the performance map. Using full wheel unsteady computation on a turbocharger compressor, Dickmann et al [12] observed that the bleed flow is interrupted by the impeller main blades passing by resulting in alternating maxima and minima of pressure and flow velocity, and the non-axisymmetric elbow and volute tongue have significant influence on the circumferential pressure distribution of the rotating impeller, leading to unsteady main blade power.

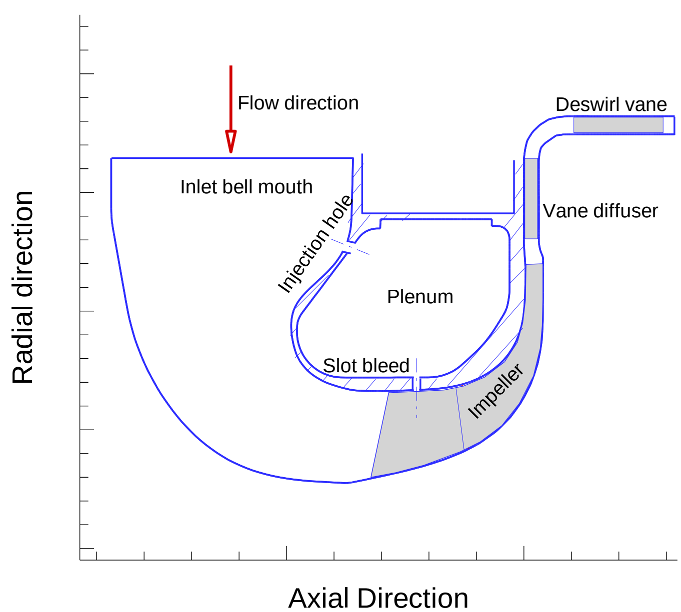


Fig. 1 Layout of ported shroud configuration for research compressor application

## Objectives

It can be seen that most of research on ported shroud in recent years were focused on the optimization of its configuration and bleed slot geometric parameters. The compressor performance and bleed flow details were interrogated primarily by steady CFD modeling without considering unsteady interaction between the impeller blade and discrete bleed holes and/or ported shroud guide vane. Such type of unsteady interaction can introduce vibratory forcing to the compressor blade at a frequency dependent on the relative blade and bleed hole counts and sometimes results in compressor blade damage. Unsteady interaction can also occur between the reinjected air flow and the bow wave of transonic impeller leading edge. Though Dickmann et al [12] investigated the unsteady interaction between bleed flow and main flow, how its separate impacts on blade loading without taking account of non-axisymmetric suction elbow effects are not identified and still remain unclear. Therefore, it is desired that by understanding the flow physics of such unsteady interactions, the design parameters for non- axisymmetric bleed holes or ported shroud guide vane can be well identified. To achieve this goal, the present paper will be focused on the study of transient bleed flow behavior and unsteady blade loading for a single stage, high pressure ratio centrifugal compressor, where non-axisymmetric bleed holes and injection holes are circumferentially uniformly arranged on the inducer and inlet bellmouth shroud. The specific questions that will be addressed are as follows.

1. What is the performance benefit or penalty of having a shroud bleed? What is the performance map difference between modeling the bleed as axisymmetric/steady state vs. unsteady?
2. What does the bleed do to the incidence angle that the main blade and the splitter blades see?
3. What does the bleed do to the time-average blade loading? How does the time-average blade loading compare to the axisymmetric/steady state blade loading? How does the blade loading compare to the case without slot?
4. What does the bleed do to the unsteady blade loading? How far down the span is the unsteady blade loading "felt"?

## Approaches

Numerical methods are utilized to tackle the questions asked in the paper. Three-dimensional time-accurate simulations are able to meet the need for analyzing the transient flow behavior and the time-averaged performance. A simplified centrifugal compressor stage, comprising only impeller and vaneless diffuser, is chosen as the research target. Results are compared between the steady and unsteady simulations to identify the unsteady interaction impacts.

## PAPER ORGANIZATION

Following the introduction, a brief description is given for the basic parameters of the compressor under study and the CFD model, including the solver, turbulence model, boundary conditions and grid generation. Next, the research results are elaborated in two sections. The first section contains steady simulation results with and without bleed, in which the performance map, variance of bleed flow with operation condition, blade loading and flow field are analyzed. The second section contains the unsteady simulation results, where time-averaged performance map, bleed flow history, transient and time-averaged incidence angle and blade loading are interrogated.

## NOMENCLATURE

| | |
|---|---|
| Eta | total to static adiabatic efficiency |
| PR | total to static pressure ratio |
| Wc | corrected inlet mass flow (kg/s) |
| Wc' | inlet corrected mass flow normalized by the inlet mass flow at peak efficiency, without bleed |
| P | static pressure [Pa] |
| Pt | total pressure [Pa] |
| ρ | air density |
| U | rotational velocity [m/s] |
| Δβ | flow incidence angle [deg] |
| RPM | rotation speed per minutes |
| Qtip | $= 0.5\rho_1 U_2^2$ |
| $\overline{M}_{inlet}$ | time-averaged mass flow rate at intake [kg/s] |
| $\overline{M}_{bleed}$ | time-averaged bleed mass flow rate [kg/s] |
| $M_{bleed}$ | transient bleed mass flow rate [kg/s] |
| MOF | $=(M_{bleed} - \overline{M}_{bleed})/\overline{M}_{inlet}$, bleed fluctuation magnitude |

Subscript

| | |
|---|---|
| ps | Pressure surface |
| ss | Suction surface |
| 1 | impeller inlet |
| 2 | impeller exit |

## DESCRIPTION OF COMPUTED COMPRESSOR AND CFD MODEL DETAILS

### Description of the Compressor

A cross-section view of the baseline compressor under study is shown in Fig. 1. The stage primarily comprises an inlet bellmouth, shroud bleed system, impeller, vane diffuser and exit deswirl vane. The shroud bleed system consists of settling plenum, 10 bleed holes and 24 injection holes. These bleed and injection holes are discretely spaced around the shroud circumference in uniform space. The impeller is a state-of-the-art design with the pressure ratio of 8:1, including 16 main blades and 16 splitter blades. The number of diffuser vanes and deswirl vanes is 23 and 51, respectively. The design rotating speed is 51,500 RPM.

### CFD Model Details

The original compressor stage has been simplified to avoid a full wheel unsteady computation. The diffuser vane and deswirl vane were replaced by a vaneless diffuser. The bleed holes were scaled from 10 to 8 in number while keeping identical total bleed open area and streamwise location of the hole center, so that the ratio of injection hole number to bleed holes number to impeller main blades number is changed from 12:5:8 to 3:1:2. With this scaling, the assumption is made that although the absolute interaction frequencies between the impeller blade and shroud bleed holes are modified, the magnitude of the unsteady effects is not. The final computation domain based on these simplifications is illustrated in Fig. 2, which consists of 45 deg. sector of inlet bellmouth and bleed plenum, three injection holes, one bleed hole, two main blade/splitter blade passages and 45 deg. sector of vaneless diffuser.

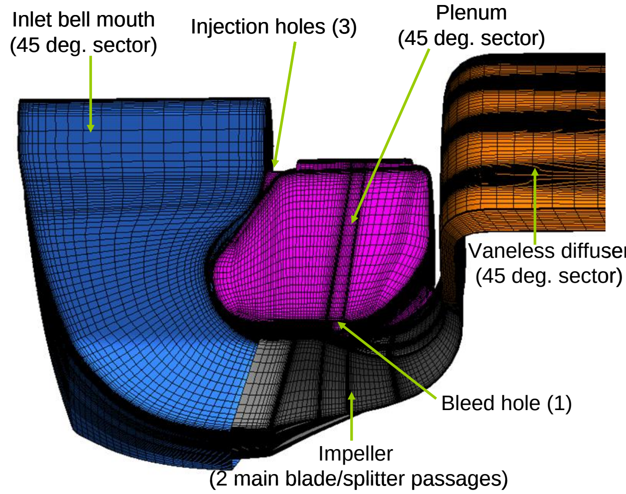


Fig. 2 Computational model of APS4900

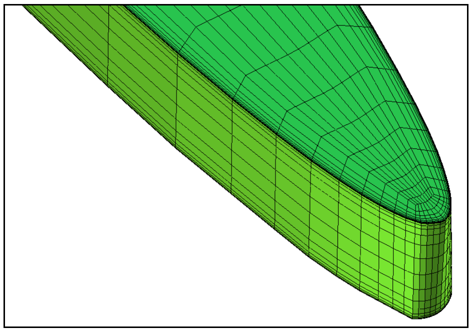

Fig. 3 impeller tip gap grid topology and distribution around blade LE

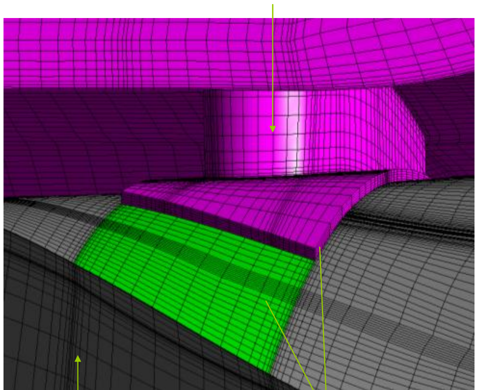

Fig. 4a Grid distribution on bleed hole surface

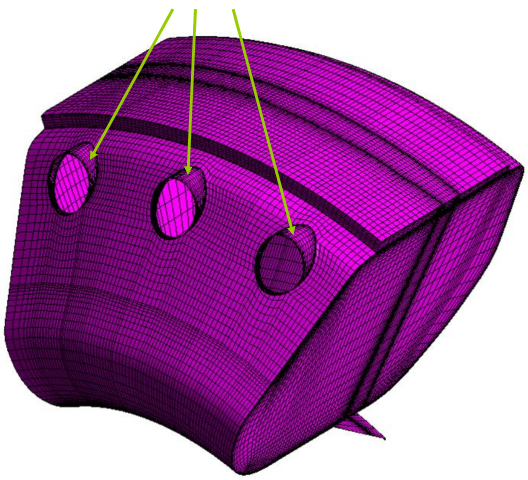

Fig. 4b Grid distribution on plenum and reinjection hole surface

The commercial CFD software, ANSYS CFX 11, is chosen for the current study. CFX is a three-dimensional, time-accurate, viscous solver implementing a second order accurate finite volume scheme to solve the unsteady Reynolds-averaged Navier-Stokes equations. One impeller main blade pitch is resolved by 60 time steps, which means that the chosen number corresponds to 0.375° turning of impeller per time step. Within each time step, 10 inner loops are executed to enable the maximal residual reduces to less than $10^{-3}$. The turbulence model selected is the standard K-Omega model. Automatic wall functions are applied to allow for an automatic switch between wall-function and low-Re near wall formulations for different local y+ values. The interfaces between stationary and rotating components are computed using CFX's "sliding" interface model (between inlet bellmouth and impeller; between impeller and vaneless diffuser; and between shroud bleed hole and impeller).

Besides the unsteady computation with non-axisymmetric bleed hole, a steady computation with an axisymmetric bleed slot was also executed to help understand how the bleed flow impacts the compressor performance when a steady flow assumption is made. The axisymmetric bleed slot has the same open area as the original discrete bleed holes, as well as the same central streamwise location. In the steady state computations, "stage" interfaces, based on a mixing plane method, are used instead of "sliding" interfaces.

The total pressure, total temperature and normal flow direction at sea level are specified uniformly at the inlet boundary with 5% turbulence intensity and viscosity ratio of 100. No-slip and adiabatic conditions are imposed on all the solid walls. To obtain the speedline characteristics of compressor, the static pressure is specified at outlet boundary and gradually increased to move the operation point from choke to lower flow rate. Once approaching the near-stall point, the mass flow rate rather than static pressure is specified at outlet boundary. The speedline is calculated to progressively lower mass flows until a converged solution is no longer achievable. Steday-state computations are not suitable for the proper detection of the flow instability onset found at the surge line, as this phenomenon is an inherently unsteady process.

For grid generation, hexa meshes were generated using ICEM-CFD for the entire computational domain with the total grid number of approximately 1.9 million. The mesh topology and resolution of each component are shown in Fig. 2. The zoomed grid details around the impeller tip gap, the bleed hole and injection hole, as well as the plenum surface, are shown in Fig. 3 and 4. It is seen that the mesh is a multiblock structured grid. For the impeller tip gap, the gap size is 0.008 inch, uniform from the impeller leading edge to trailing edge, with 15 grid nodes generated in the tip height direction. The resultant area averaged Y+ values are 0.3 ~ 1.8 for impeller, 4.1 ~ 17.4 for the diffuser, and 8.0~23.2 for bellmouth and plenum.

## RESULTS OF STEADY SIMULATION WITH AND WITHOUT BLEED

### Performance Map With and Without Bleed

The predicted overall performance of compressor stage with and without bleed by steady computation is shown in Fig. 5 and 6. The results are nondimensionalized by the values at the peak efficiency point without bleed. It is seen that the bleed flow results in a 6.9% increase in the choke flow rate and a 7.9% decrease in stall point flow rate, and thereby the total operation range is broadened compared to the case without bleed. In contrast to the range extension, the bleed flow causes a decrease of total-to-static adiabatic efficiency over the entire operating range and a decrease of pressure ratio in high mass flow operation. At the peak efficiency point, the efficiency penalty due to the bleed flow is about 1%, and the pressure ratio penalty is about 2.5%. The efficiency penalty over the entire operating range can be ascribed to the additional loss of the recirculating bleed flow in the settling plenum, which is further explained in the following section.

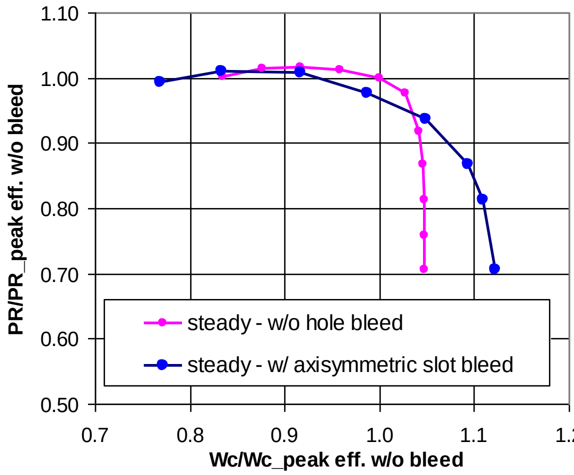


Fig. 5 Pressure ratio versus flow rate map with and without bleed predicted by steady computation

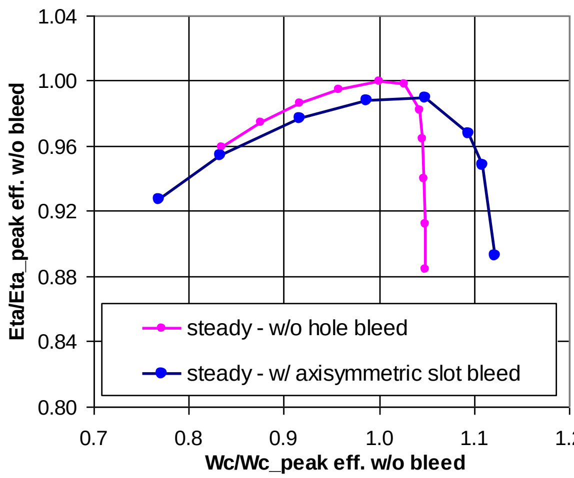


Fig. 6 Efficiency versus flow rate map with and without bleed predicted by steady computation

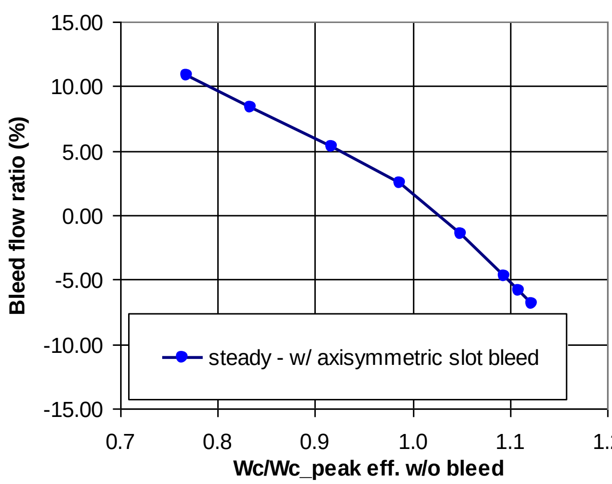


Fig. 7 Variation of bleed flow ratio with operation conditions

**Effects of Operation Condition on Bleed Flow**

The variation of bleed flow rate with operating condition is illustrated in Fig. 7, where the ratio of bleed mass flow rate to the compressor inlet mass flow rate is plotted versus normalized inlet corrected flow. It is noted that the bleed flow ratio increases monotonically from negative values at choke to positive values at the near-stall point. The bleed slot is located downstream of the impeller throat, so that at choke, when there is lower inducer shroud pressure than the inlet pressure, the air inflow is forced from bellmouth injection hole through the settling plenum and out the shroud bleed slot. At lower inlet mass flow operating points, the inducer shroud pressure increases due to the successive increase in inducer loading, and once it exceeds the inlet pressure, the air is bled out of inducer and into the settling plenum, resulting in the positive bleed flow ratio. Moreover, by checking the bleed flow ratio for the peak efficiency point from Fig. 6 and Fig. 7, it is seen that the peak efficiency point occurs near the zero bleed flow condition, which is consistent with the results from studies conducted by both Yin et al [8] and Tamaki et al [11]. The peak efficiency point is at close to zero bleed flow because zero bleed flow is the minimum recirculating flow loss.

The structure of the bleed flow, as represented by 3d streamlines, is shown in Fig. 8a and 8b for the choke and near-stall point, respectively. As we expect, air inflow to the settling plenum appears at choke condition (negative bleed flow ratio), and air outflow arises at near-stall condition (positive bleed flow ratio). The flow in the settling plenum forms a strong recirculation area.

**Effects of Bleed Flow on Impeller Blade Loading**

The impacts of bleed flow on blade loading are evaluated through Fig. 9, where the normalized loading at 97% span is plotted for the near-stall condition. The axisymmetric bleed slot covers 0.151 to 0.175 streamwise location, marked by the red dashed lines in the figure. For the main blade, the introduction of bleed flow results in approximately 35% decrease in the loading upstream of the bleed slot while about 5% decrease downstream of the bleed slot. This implies that the bleed flow impacts the forward part loading of the blade much more than the rearward. The loading reduction upstream of the slot can be ascribed to the mitigation of leading edge incidence angle; because the bleed air is reinjected upstream of the impeller leading edge, it increases the local flow rate in the tip region and reduces the blade incidence. Detailed analyses on the incidence angle distribution are discussed in the section describing the unsteady simulation. A loading increase is seen for the splitter blade, but it is small in comparison with the main blade. What should be emphasized is the sharp loading jump right under the bleed slot, which is due to the fast pressure increase across the slot on main blade pressure surface. In reality, the blade loading will always change with different relative locations of impeller blade to the discrete bleed holes.

 

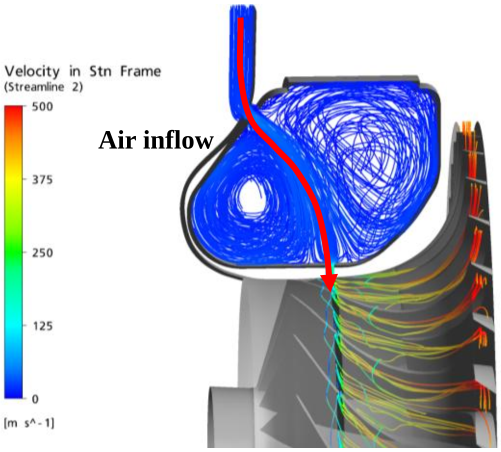


(a) Choke point

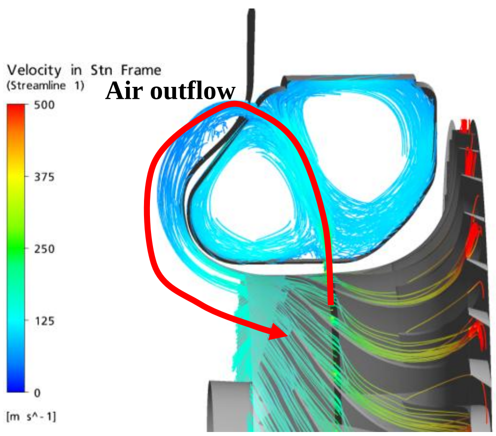


(b) Near-stall point

Fig. 8 3D streamline of bleed flow at choke and near-stall point

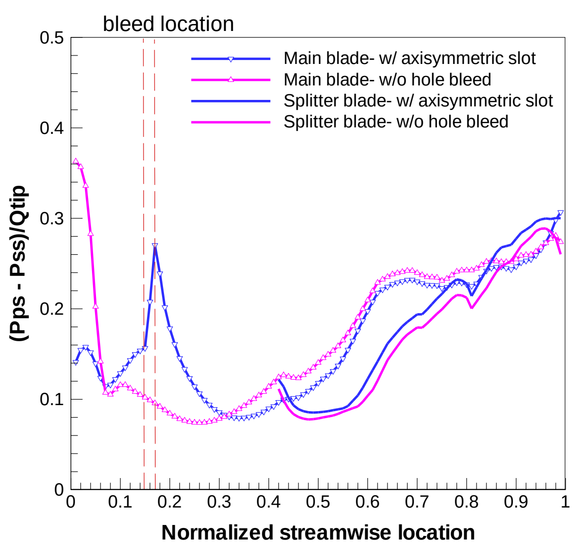


Fig. 9 Streamwise distribution of blade loading at 97% span at near-stall point

## Effects of Bleed Flow on Flow Structures in Impeller

Bleed flow causes very different flow patterns in the impeller tip region at near stall point, as shown by the relative Mach number contour at 97% span in Fig. 10. The dashed line in the figure represents the trajectory of the tip vortex. The lower Mach number region in the inducer passage, caused by the tip vortex, is mitigated by bleed flow. The intersection point between the tip vortex trajectory and the neighboring blade is pushed downstream and farther away from the leading edge, which indicates that not only the inducer blade loading is reduced, but also the stall margin is extended according to the stall inception study by Huu Duc Vo [13]. As discussed earlier, the reinjected bleed air enhances the local flow rate in the tip region, thus reducing the excessive incidence angle and delaying inducer stall. Moreover, by checking the value of Mach number before the leading edge shock, it can be noted that the bleed flow reduces the Mach number about 10% in front of the shock. Consequently, the shock loss decreases as well.

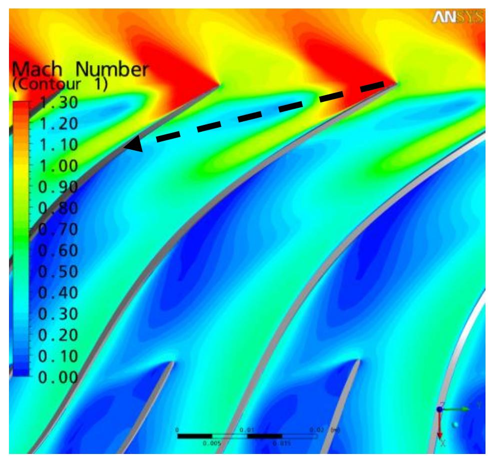


(a) Without bleed

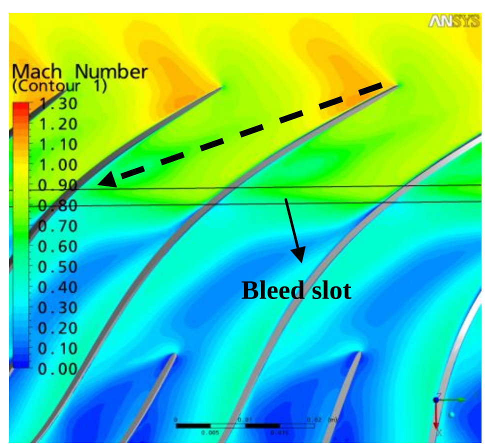


(b) With axisymmetric slot

Fig. 10 Relative Mach number contour at 97% span for near-stall operating point

## RESULTS OF UNSTEADY SIMULATION WITH BLEED

The next several sections are focused on the interrogation of unsteady simulation results. The unsteady analyses for the near-stall point are emphasized, since the bleed flow is much stronger at near-stall than at the peak efficiency point.

### Performance Map

The time-averaged performance at near-peak efficiency and a near-stall point, in comparison with the steady solution, is plotted in Fig. 11 and 12. It is seen that the unsteady results are similar to the steady prediction, and therefore it can be concluded that representing the bleed flow as axisymmetric, hence steady state in the rotating frame of reference, provides adequate assessment of the time-average compressor performance.

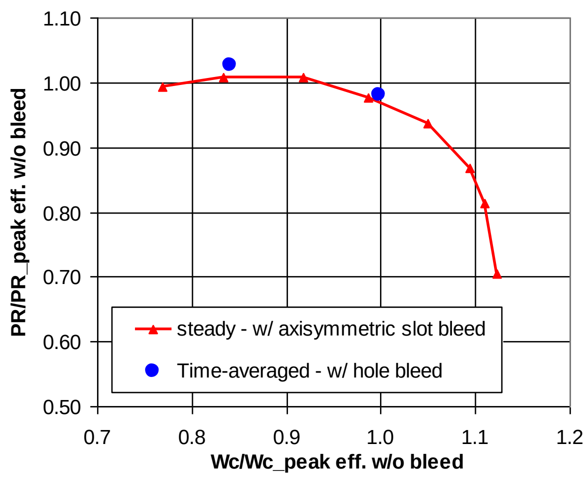


Fig. 11 Comparison of pressure ratio performance between steady solution and time-averaged unsteady solution

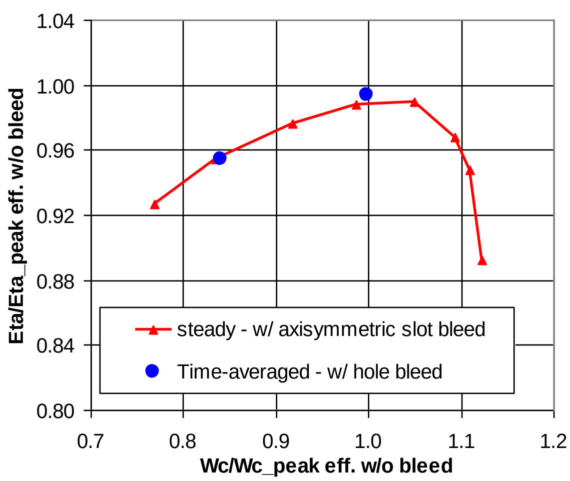


Fig. 12 Comparison of efficiency performance between steady solution and time-averaged unsteady solution

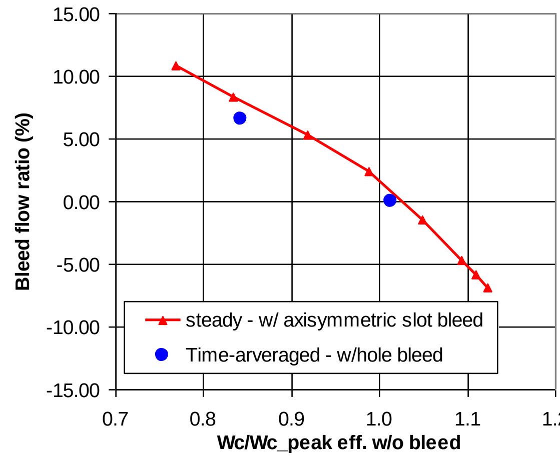


Fig. 13 Comparison of bleed flow ratio between steady solution and time-averaged unsteady solution

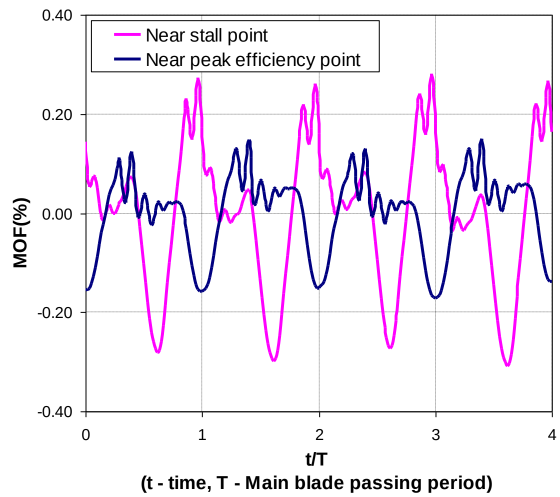


Fig. 14 Time history of bleed air fluctuation, origin arbitrary

### Time-averaged and transient bleed flow ratio

The time-averaged bleed flow ratio is illustrated in Fig. 13. The comparison with the steady solution shows that the unsteady computation predicts a 1.8% smaller bleed flow ratio than the steady computation at both operating points considered.

The transient fluctuation of bleed flow ratio is shown in Fig. 14, where MOF is defined as the transient bleed flow rate minus the time-averaged value and then normalized by the time-averaged intake flow rate of bellmouth. The bleed flow takes on periodic fluctuation at blade passing frequency (BPF) for both the near-peak efficiency and near-stall point. The fluctuation magnitude at the near-stall point is within ±0.3% of time-averaged intake flow rate and within ±0.15% at the near-peak efficiency point. Since the time-averaged bleed flow ratio is around 7% and 0% at near stall and peak efficiency point, respectively, the bleed flow ratio is always positive at near-stall while alternating between the positive and negative value at near-peak efficiency point.

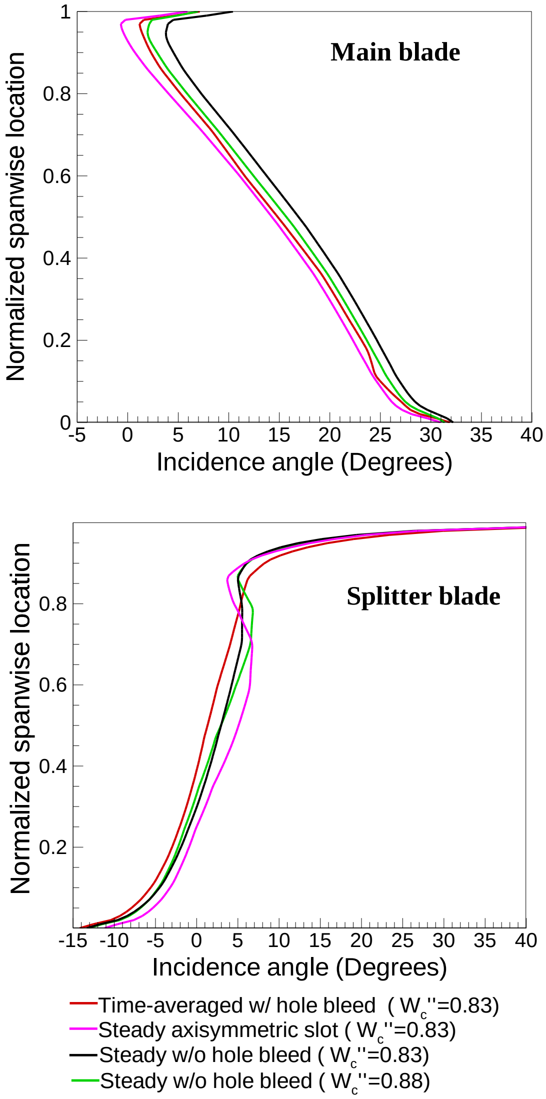


Fig. 15 Comparison of incidence angle between time-averaged and steady solution at near-stall point

**<u>Analysis of Time-averaged and Transient Incidence Angle</u>**

The spanwise distribution of time-averaged incidence angle at near-stall point is shown in Fig. 15. As a comparison, the steady solutions with and without bleed, for the same inlet mass flow, are also shown. The normalized inlet corrected flow Wc' is used here for easy description of the operating condition. For the fixed Wc'=0.83 (near-stall point) at bellmouth intake, both time-averaged and steady solution show the reduction of main blade incidence angle along the entire span, and moreover, the tip region has higher reduction than other regions. The steady solution with axisymmetric slot bleed predicts the maximum incidence angle reduction due to the higher bleed flow ratio at near-stall point, as seen in Fig. 13. Accounting for the additional throughflow associated with the injection of bleed air, the actual mass flow rate passing through impeller inducer in the case of Wc'=0.83 with bleed is equivalent to the case of Wc'=0.88 without bleed. Therefore, the time-averaged incidence angle distribution at Wc'=0.83 looks very similar to that at Wc'=0.88 without bleed, which is also plotted. The higher incidence angle arising around main blade hub region is because the current simulation result is based on 95% design speed, not the design speed.

For the splitter incidence angle distribution, it is difficult to see the benefit of bleed flow in improving the flow in the splitter tip region because the bleed hole is upstream of the splitter leading edge, and the local flow rate is reduced when reaching the splitter blade. Due to the blockage of tip vortex flow originated from the inducer, a higher incidence angle distribution arises at the splitter tip region.

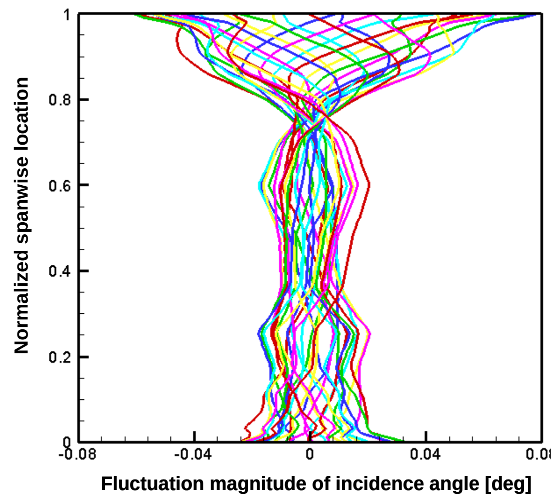


(a) Main blade

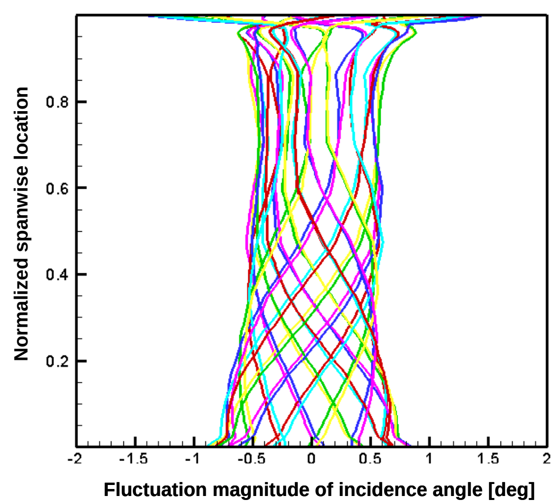


(b) Splitter blade

Fig. 16 Fluctuation magnitude of incidence angle along spanwise direction at near-stall point.

The periodic variation of bleed flow rate leads to a fluctuating incidence angle. Fig. 16 plots the fluctuation magnitude of incidence angle as a function of span, at different time steps for the near-stall point. Both main blade and splitter blade experience incidence angle fluctuation from hub to shroud, and comparatively, the outer 10% span produces a higher fluctuation magnitude, approximately ±0.08 deg. for main blade and ±1.0 deg. for splitter blade.

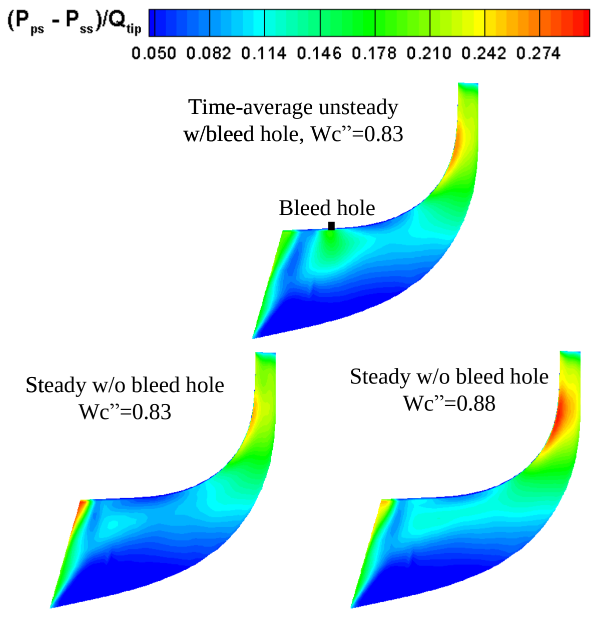


Fig. 17 Normalized loading distribution on the main blade near-stall point

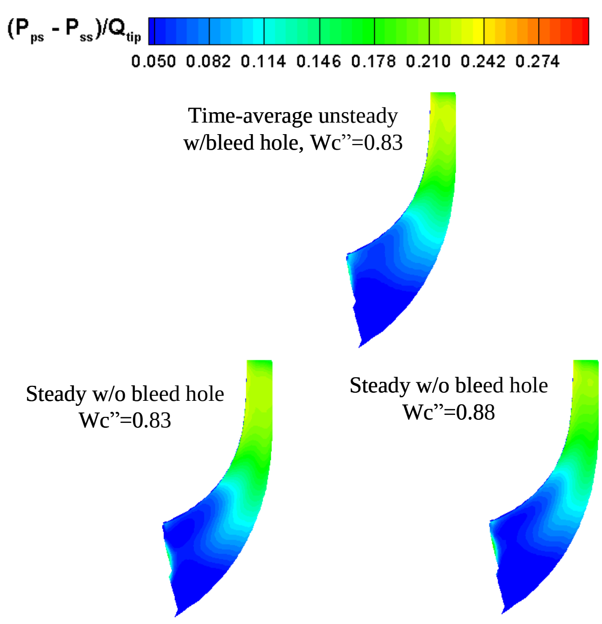


Fig. 18 Normalized loading distribution on splitter blade near-stall point

## Analysis of Time-averaged and Transient Blade Loading

Fig. 17 and 18 show the time-averaged blade loading distribution on the main and splitter blades at the near-stall condition. The time-averaged solution exhibits a loading jump at the location right under the bleed hole, which is consistent with the axisymmetric slot bleed results shown in Fig. 9. Compared to the steady solution without bleed at Wc'=0.83 (near-stall point), the time-averaged loading differs primarily at the leading edge due to the local reduction in incidence angle. Compared to the steady solution without bleed at Wc'=0.88, which has the same mass flow rate at the impeller leading edge, the time-averaged loading differs over the outer half of the blade. The splitter blade loading distribution does not show a significant difference between the time-averaged solution and the steady solutions, and therefore it can be concluded that the bleed flow make less impact on the splitter blade than it does to the main blade, when the bleed hole is well upstream of the splitter leading edge.

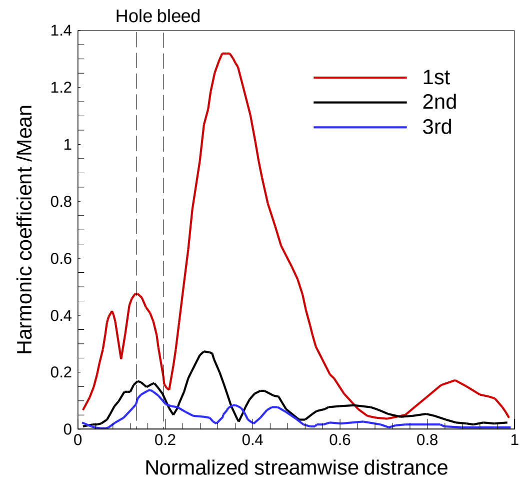


Fig. 19 Harmonic blade loading at 97% span of main blade at near-stall point

Harmonic analysis was performed to reveal the impact of bleed flow on the unsteady blade loading. The bleed hole passing frequency is half of blade passing frequency (BPF) since there are two main blades for each bleed hole. The harmonic numbers described here refer to hole passing frequency. First, the harmonic blade loading at 97% span of main blade is plotted in Fig. 19 for the near-stall point, which shows that the unsteady blade loading is dominated by the first and second harmonic of bleed hole passing frequency. Fig. 19 also shows that the large loading variation occurs downstream of the bleed hole rather than under the bleed hole. To understand further how the unsteady blade loading changes in the spanwise direction, the first and second harmonic loading distributions are plotted on the entire main blade and splitter blade surface at the near-stall condition in Fig. 20 and 21. Similar to Fig. 19, large first harmonic loading is observed downstream of the bleed hole that extends as far down as 60% span of the main blade, with similar magnitude as the mean loading. The large first harmonic loading also arises at lower span close to the hub, which is probably due to reflection. In contrast to the first harmonic loading, the second harmonic main blade loading distribution is much reduced. On the splitter blade, the first and second harmonic loading are small and more uniform along the entire span, and the large loading variation mainly occurs at the exducer section. In sum, the harmonic loading analysis indicates that the unsteady interaction between impeller blade and bleed hole causes quite large loading fluctuation downstream of the bleed hole, which needs to be accounted for in the mechanical design.

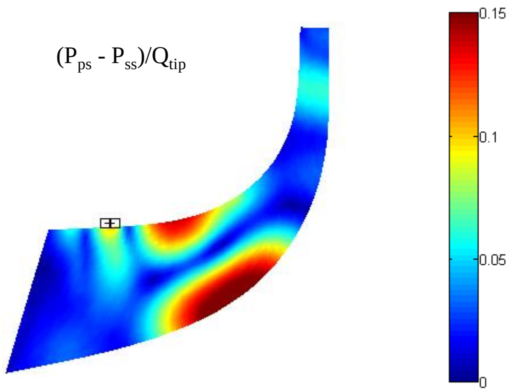


(a) 1st Harmonic

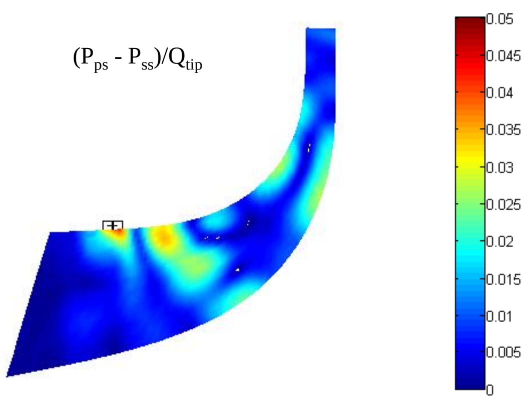


(b) 2nd Harmonic

Fig. 20 Harmonic loading of main blade at near-stall point

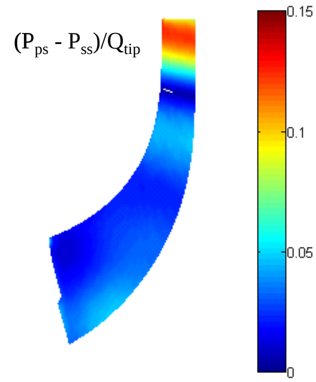


(a) 1st Harmonic

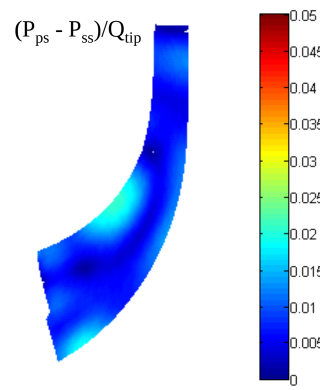


(b) 2nd Harmonic

Fig. 21 Harmonic loading of splitter blade at near-stall point

## CONCLUSIONS

Time-accurate simulations of the flow through a centrifugal compressor stage consisting of a radial inlet with air injection holes, an impeller with shroud bleed holes, and vaneless diffuser were performed to reveal the impact of unsteady interaction between bleed hole and impeller blade on compressor performance. The time-averaged and transient flow solutions were compared with the steady solutions without bleed and with axisymmetric slot bleed. The following conclusions can be drawn.

1. The steady solutions based on axisymmetric bleed assumption are quite similar to the time-averaged compressor performance with hole bleed. The axisymmetric steady state model can provide useful information about the time-average performance and flow field.
2. The bleed acts to reduce the main blade incidence angle at lower mass flow conditions. The unsteady fluctuations of incidence angle to the main blade are quite small, within ±0.08 deg, but to the splitter blade can be ~±1 deg at high bleed flow rates.
3. In the presence of bleed flow, the main blade time-average blade loading is reduced in the leading edge area due to the reduced incidence angle, but overall increased for higher PR. The bleed slot is “felt” locally streamwise down to about 60% span.
4. In the presence of bleed flow, the main blade unsteady loading can be quite large, both in the region downstream of the bleed hole and through reflections to the hub area. For this configuration, the 2$^{nd}$ harmonic of hole passing frequency (which is BPF) is much smaller than the 1$^{st}$ harmonic.

## ACKNOWLEDGMENTS

The authors would like to thank Dr. Om Sharma, UTRC senior fellow, for his technical guidance and dedicated effort to this project.

## REFERENCES


[1]. Rodgers, C., 2005. "Flow Ranges of 8.0:1 Pressure Ratio Centrifugal Compressors for Aviation Applications", ASME GT2005-68041.

[2]. Salvage, J. W., 1997, “Variable Geometry Pipe Diffusers”, ASME Journal of Turbomachinery, Vol. 119, No.4, pp. 831-838.

[3]. Salvage, J. W., 1997, “Development of a Centrifugal Compressor with a Variable Geometry Split-Ring Pipe Diffuser”, ASME Journal of Turbomachinery, Vol. 121, No.2, pp. 295-304.

[4]. Skoch, G.J., 2004. “Experimental Investigation of Diffuser Hub Injection to Improve Centrifugal Compressor Stability”. ASME GT2004-53618.

[5]. Barton, et al., 2004, “Numerical Optimization of a Vaned Shroud Design for Increased Operability”, ASME GT2004-54287.

[6]. Fisher, F.B., 1988, “Application of Map Width Enhancement Device to Turbocharger Compressor Stages”, SAE Paper No.880794.

[7]. Slovisky, J., et al., 2005. “Numerical Design Experiment to Optimize a Ported Shroud to Extend Operability Margin of a Centrifugal Compressor”, ASME GT2005-68870.

[8]. Yin, J., Li, P., and Pees, S., 2009, “Optimization of Turbocharger Ported Shroud Compressor Stages”, ASME GT2009-59248.

[9]. Ishida, M., Sakaguchi, D and Ueki, H., 2005. “Optimization of Inlet Ring Groove Arrangement for Suppression of Unstable Flow in a Centrifugal Impeller”, ASME GT2005-68675.

[10]. Ishida, M., Sakaguchi, D and Ueki, H., 2006. “Effect of Pre-whirl on Unstable Flow Suppression in a Centrifugal Impeller with Ring Groove Arrangement”, ASME GT2006-90400.

[11]. Tamaki, H., Unno, M., and Kawakubo, T., 2009. “Aerodynamic Design to Increase Pressure Ratio of Centrifugal Compressors for turbochargers”, ASME GT2009-59160.

[12]. H.P. Dickmann, T.S. Wimmel, J. Szwedowicz, D. Filsinger, C.H. Roduner, 2006, “Unsteady Flow in a Turbocharger Centrifugal Compressor: Three-Dimensional Computational Fluid Dynamics Simulation and Numerical and Experimental Analysis of Impeller Blade Vibration”. J. Turbomachinery, Vol. 128, No. 3, 455-465.

[13]. Huu Duc Vo, 2001. “Role of Tip Clearance Flow on Axial Compressor Stability”, PhD Thesis, MIT Department of Aeronautics and Astronautics.